Spontaneous Growth and Phase Transformation of Highly Conductive Nickel Germanide Nanowires

Chaoyi Yan,[†] Jeremy M. Higgins,[‡] Matthew S. Faber,[‡] Pooi See Lee,[†,*] and Song Jin[‡,*]

[†]School of Materials Science and Engineering, Nanyang Technological University, Singapore 639798, and [‡]Department of Chemistry, University of Wisconsin—Madison, 1101 University Avenue, Madison, Wisconsin 53706, United States

ABSTRACT We report the synthesis, phase transformation, and electrical property measurement of single-crystal NiGe and ε-Ni_5Ge_3 nanowires (NWs). NiGe NWs were spontaneously synthesized by chemical vapor deposition of GeH_4 onto a porous Ni substrate without the use of intentional catalysts. The as-grown NWs of the orthorhombic NiGe phase were transformed to the hexagonal ε-Ni_5Ge_3 phase by thermal annealing induced Ni enrichment. This controllable conversion of germanide phases is desirable for phase-dependent property study and applications, and the observation of novel metastable ε-Ni_5Ge_3 phase suggests the importance of kinetic factors in such nanophase transformations. Electrical studies reveal that NiGe NWs are highly conductive, with an average resistivity of $35 \pm 15\ \mu\Omega \cdot$cm, while the resistivity of ε-Ni_5Ge_3 NWs is more than 4 times that of the NiGe phase. NWs of nickel germanides, particularly NiGe, would be useful building blocks for germanium-based nanoelectronic devices.

KEYWORDS: nickel germanide · nanowire · phase transformation · nanoelectronics · resistivity

Germanium is an appealing alternative material for high-speed nanoelectronic and nanophotonic devices due to its high carrier mobility and compatibility with current Si-based microelectronics.[1,2] As complementary metal oxide semiconductor (CMOS) transistors continue to scale to shorter channel lengths and higher current levels, attention to proper contact materials becomes crucially important to minimize series resistance and achieve high performance.[1,3] Transition metal germanides are the natural candidates for contacting and interconnecting Ge and have been intensively studied.[1,3−6] In particular, nickel monogermanide (NiGe) exhibits a number of superior properties compared with other germanides, including low resistivity, low formation temperature, a wide temperature stability window, and facile chemical processing;[1,7] therefore, it is the most commonly used germanide in Ge-based devices.[1,3,7,8] Nanoelectronic devices built with Ge nanowires (NWs) have demonstrated high performance.[9,10] For Ge-based nanoelectronics, nanoscale metal germanides could be the natural contact and/or gate materials.[5] Despite extensive studies on the formation and properties of nickel germanides in bulk or thin films,[1,7,8,11,12] there has been no report thus far on the synthesis and property investigation of one-dimensional (1D) nickel germanide NWs.

In the context of their formation and nanoelectronic applications, NWs of metal germanide can be compared to NWs of silicides. NWs of many silicides have been synthesized *via* bottom-up strategy and used as robust building blocks in a number of applications.[13] The one-dimensionality of the NW morphology coupled with the unique properties of silicides makes them ideal candidate materials for application in field emission,[14,15] thermoelectrics,[16,17] spintronics,[18,19] and self-aligned metallic gates in graphene transistors.[20] Controlling the stoichiometric composition and crystallographic phase of silicide and germanide NWs is rather difficult due to the complex phase formation behavior. The Ni−Si binary system is fairly well studied with six equilibrium phases and five metastable phases.[21] Every equilibrium nickel silicide phase ($NiSi_2$,[22] NiSi,[14,23−26] Ni_3Si_2,[27] Ni_2Si,[25,28−30] $Ni_{31}Si_{12}$,[31] and Ni_3Si[32,33]) has been synthesized in the NW morphology, but little is known about why a certain phase is obtained under specific conditions, that is, whether the NW growth is governed by diffusion or other kinetically limited processes. The Ni−Ge binary system is less studied but displays similar complexity,[11] including four equilibrium phases (NiGe, ε'-Ni_5Ge_3, Ni_2Ge, and Ni_3Ge) and five metastable phases (Ni_3Ge_2, $Ni_{19}Ge_{12}$, ε-Ni_5Ge_3, δ-Ni_5Ge_2, and γ-Ni_3Ge) (Figure S1, Supporting Information).[34] In fact, controversy surrounds the phase field between NiGe and Ni_2Ge, which consists of ε'-Ni_5Ge_3, Ni_3Ge_2, $Ni_{19}Ge_{12}$, and ε-Ni_5Ge_3,[35] all variants of the

* Address correspondence to pslee@ntu.edu.sg, jin@chem.wisc.edu.

Received for review March 23, 2011 and accepted May 3, 2011.

Published online May 03, 2011
10.1021/nn201108u

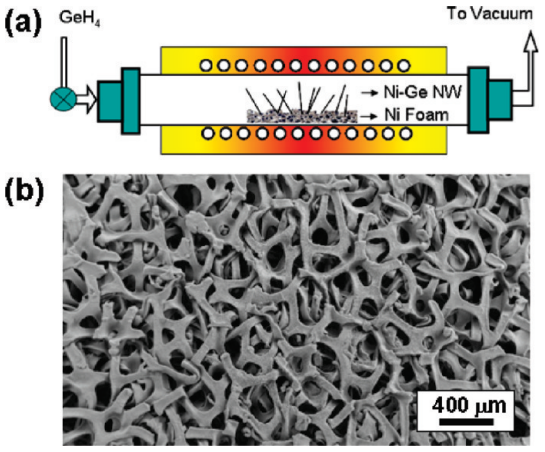

Figure 1. (a) Schematic diagram highlighting the CVD reaction of GeH_4 with a porous Ni foam substrate to form nickel germanide NWs. (b) Low-magnification scanning electron microscopy (SEM) image of the porous Ni substrate before reaction.

same parent B8 structure and often collectively referred to as "Ni_5Ge_3". These related phases are not easily distinguished using X-ray diffraction (XRD) techniques (Figure S2, Supporting Information) and therefore typically require careful single-crystal XRD or electron diffraction (ED) investigations for explicit phase identification. Such complex phase behavior is common among germanides and likely contributes to the scarcity of NW reports—only NWs of selected phases of manganese germanides[36] (as part of syntaxial growth of Ge NWs), cobalt germanides,[15] and an iron silicide–germanide alloy[37] have been reported to our knowledge. Such complexity also makes phase-controlled formation of silicide/germanide NWs rather difficult. Yet such control is highly desirable in order to investigate their phase-dependent properties and explore their applications. Nickel germanide NWs with low resistivity would be attractive contact materials in nanoelectronics or high-performance field emitters.

In this paper, we report the facile synthesis and structural characterization of NiGe NWs for the first time. Further, the successful phase transformation from NiGe to ε-Ni_5Ge_3 NW was demonstrated by thermal annealing induced Ni enrichment. We further investigate their phase-dependent transport properties, finding the resistivity of ε-Ni_5Ge_3 NWs to be more than 4 times that of the NiGe phase. The strongly phase-dependent electrical properties further underscore the importance of phase control from the perspective of practical applications.

RESULTS AND DISCUSSION

The NiGe NWs were synthesized by pyrolyzing GeH_4 over Ni foam substrates in a home-built chemical vapor deposition (CVD) system (Figure 1a).[19,38] Macroporous Ni foam (Figure 1b), a low-cost, commercially available material, serves as an ideal substrate for NW growth due to its high surface area. Porous substrates with functional materials grown on the surface can be highly desirable for applications where a high surface area facilitates full utilization of the active materials, such as electrochemical energy storage.[39] NWs grew spontaneously from the Ni foam substrates in these CVD reactions without the use of an intentional catalyst. The best NW morphology was obtained at a growth temperature of 350 °C and a pressure of 4 Torr.

Various growth temperatures (300–400 °C) and pressures (4–15 Torr) leading to morphological evolution of the nanostructures were investigated (Figure 2) in order to better understand the NW growth process and obtain high-quality nickel germanide NWs (*i.e.*, with uniform diameter and relatively high density). At a growth temperature of 300 °C and pressure of 15 Torr, NWs were occasionally observed on the substrate, but the density was very low (Figure 2a). We attribute the low NW density to limited GeH_4 decomposition at 300 °C. GeH_4 is a common vapor precursor for vapor–liquid–solid (VLS) growth of Ge NWs,[40–42] which was generally carried out in the temperature range of 275–320 °C to suppress NW tapering by uncatalyzed Ge sidewall deposition.[40–42] In our case, CVD synthesis at a temperature of 300 °C leads to a low NW density likely due to limited nucleation, although this condition does produce sparse NWs with uniform diameters (Figure 2a). Increasing the growth temperature to 350 °C to enhance GeH_4 decomposition results in dramatically increased nanostructure density but simultaneous increase in nonspecific sidewall deposition to yield nanocones (Figure 2b). Lowering the total system pressure helped to suppress the sidewall deposition and obtain NWs in high density and with uniform diameters, with the best results obtained at a temperature of 350 °C and a pressure of 4 Torr (Figure 2c). Attempts to increase the NW density by further raising the temperature led to much higher GeH_4 decomposition rates and resulted in thin film deposition (Figure 2d).

We have carried out detailed structure and phase analyses of the as-grown NWs produced under the best conditions (Figure 2c) and determined that these NW products of interest have the NiGe phase (Figure 3). The characterizations of the nanocones seen in Figure 2b, which are mostly made of Ge, are shown in Figure S3 in the Supporting Information. Energy-dispersive spectroscopy (EDS) of an individual NW (Figure 3e) indicates that the NW is composed of Ni, Ge, and O. The small O peak likely originates from the surface GeO_x layer visible in the transmission electron microscopy (TEM) image (Figure 3d). Peaks of Cu and Al come, respectively, from the Cu grid and Al stage used for EDS analysis. Compositional analysis of eight NWs revealed an average Ni atomic percentage of 53 ± 1%, with the most probable phase being NiGe. Furthermore, ED patterns taken along two different zone axes of the

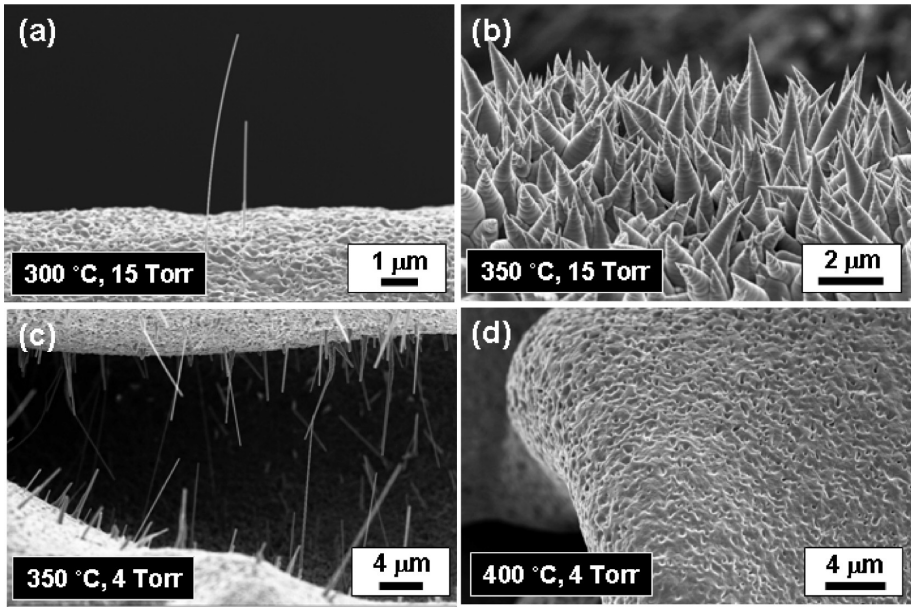

Figure 2. Optimization of the nickel germanide NW growth. (a) NW density was very low when growth was performed at 300 °C and 15 Torr, due to the limited GeH_4 decomposition. (b) When the growth temperature was increased to 350 °C, dense, tapered NWs were observed. (c) Reduction of the system pressure to 4 Torr while maintaining a growth temperature of 350 °C resulted in a high density of NWs with uniform diameters. (d) No NWs were observed when the temperature was further increased to 400 °C.

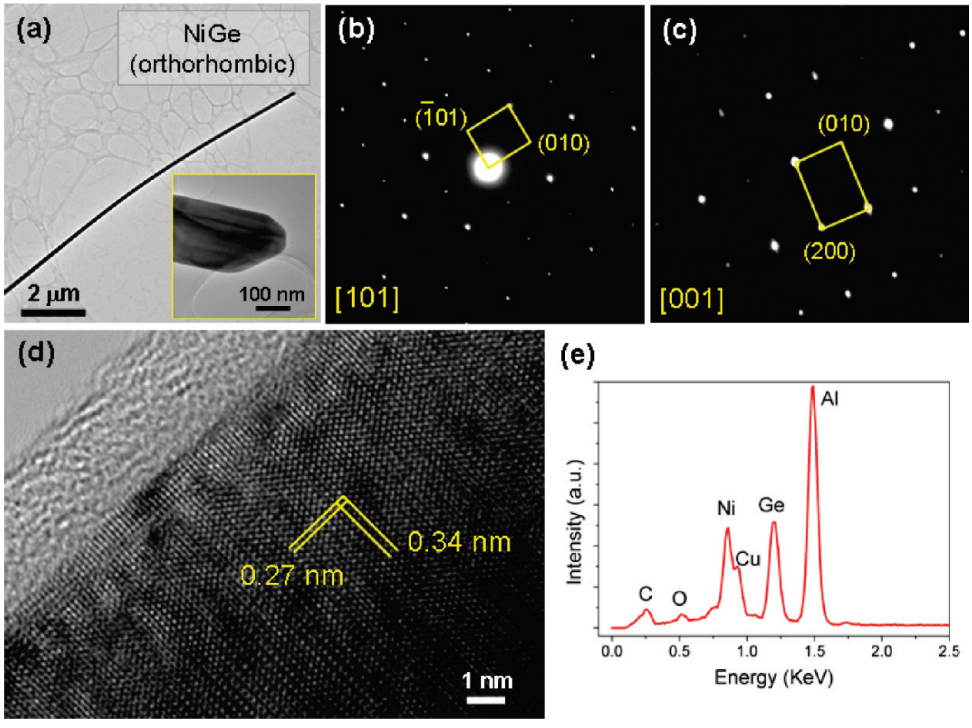

Figure 3. Structural characterizations of the as-grown nickel germanide NWs with orthorhombic NiGe phase. (a) Low-magnification TEM image (inset is a typical magnified view of NW tip), ED patterns taken along (b) [101] and (c) [001] zone axes, (d) HRTEM image and (e) EDS spectrum of the NiGe NWs.

NW (Figure 3b,c) agree with the standard ED patterns along the [101] and [001] zone axes of the orthorhombic NiGe structure (space group *Pnma*; a = 5.381 Å, b = 3.428 Å, c = 5.811 Å). The ED patterns and the lattice-resolved high-resolution TEM (HRTEM) image (Figure 3d) clearly show that these NWs are single-crystalline. Measured lattice spacings (both from the calibrated ED pattern and HRTEM image) of 0.27 and 0.34 nm correspond to the (200) and (010) planes of orthorhombic NiGe, respectively.

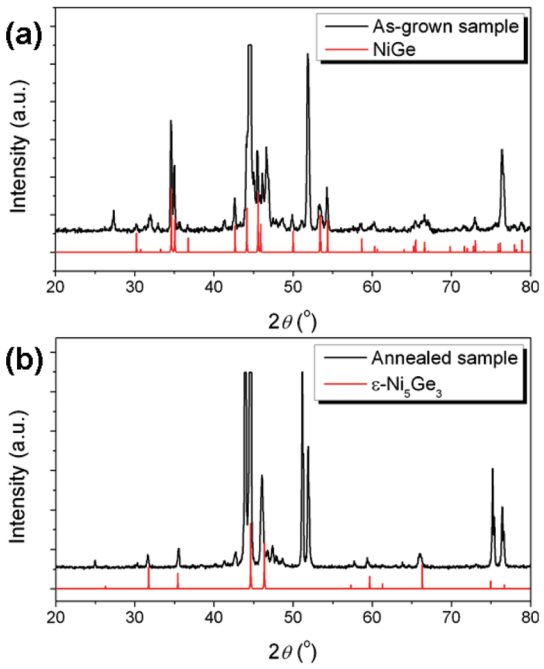

Figure 4. XRD patterns from the samples (a) before and (b) after annealing. The red lines indicate the standard diffraction peaks for (a) orthorhombic NiGe and (b) hexagonal ε-Ni_5Ge_3 phases. The completely indexed XRD patterns are shown in Supporting Information.

We have also used XRD to characterize the phases of the as-grown samples. The representative XRD pattern of the as-grown sample (Figure 4a, black curve) is compared to the standard diffraction pattern of orthorhombic NiGe (red curve) to reveal the NiGe phase clearly. A complete indexing of the XRD pattern (Figure S4, Supporting Information) reveals another three phases: Ge (cubic; a = 5.6576 Å), Ni (cubic; a = 3.5238 Å), and likely ε'-Ni_5Ge_3 (monoclinic, space group $C2$; a = 11.628 Å, b = 6.737 Å, c = 6.264 Å, β = 52.11°). However, the ED patterns of the NWs we analyzed (such as those in Figure 3b,c) did not match the ED patterns of any ε'-Ni_5Ge_3 phases. Furthermore, it is unlikely that the NWs are pure Ge or Ni since both Ge and Ni are always detected during EDS analysis of all NWs examined (Figure 3e). Taken together, the results of the XRD, EDS, ED, and HRTEM analyses suggest that the as-grown NWs are of the orthorhombic NiGe phase, but there are other germanide phases (ε'-Ni_5Ge_3) and some Ge films formed on the surface of the Ni substrate.

The growth mechanism(s) of the NiGe NWs remains to be understood, but some observations and speculations can be presented below. Decomposition of GeH_4 into Ge vapor occurs at elevated temperatures, probably with the catalytic assistance of the Ni substrate.[43] Ge will react with the Ni substrate, forming nickel germanide films, particles, or potentially NW nuclei. Since the only source of nickel is the porous Ni substrate, the thin film or NW growth necessarily have to proceed with continuous Ni diffusion from the substrate to the surface or other growth front, which is rather reasonable since Ni is a well-known fast diffuser in Ge.[44] This situation is somewhat analogous to some of the previously reported nickel silicide NW syntheses, where SiH_4 is decomposed over Ni films to form NWs of selected nickel silicide phases.[14,25,28] The growth of those silicide NWs is also not completely understood, although some suggestions have been made.[13,14,25,28] It appears that the NiGe NWs do not grow *via* the common VLS or vapor–solid–solid (VSS) mechanisms[45] since the tips of the NWs never show signs of the catalytic particles (Figure 2c) that are characteristic of such catalyst-driven growth. As shown above, a low supersaturation is required to initiate 1D growth to limit the number of nucleation sites and favor high-quality NW growth (Figure 2c), as has also been observed in previous reports.[14,46] Only thin film deposition was observed when the growth was performed at conditions of high supersaturation (Figure 2d). This might hint at dislocation-driven NW growth,[47–49] but no strong supporting evidence has been observed thus far. The continuous 1D growth of NiGe needs to be maintained by preferential axial elongation with limited radial growth. It seems that Ni might diffuse to the tips of the growing NWs and interact/react with the pyrolyzed Ge species to form the germanide phase, with the interface at the tip being a much more reactive center for reasons not presently understood. However, Ge nanocones (or strongly tapered NWs) are obtained when the radial deposition rate is still relatively large (Figure 2b), and this can be effectively suppressed by reducing the vapor pressure. The observation of nanocones (Figure 2b) is in fact a strong piece of evidence for growth from the NW tip since the sidewall deposition would be thickest on the part of the NWs formed first. NiGe NWs with uniform diameters were finally obtained at the optimized growth conditions, which favored fast tip growth rate and suppressed sidewall deposition.[50]

Since the NiGe NW growth proceeds by continuous Ni diffusion from the underlying substrate to the NW tip and subsequent reaction with Ge, annealing the as-grown samples at a higher temperature should promote further Ni diffusion from the porous substrate, allowing the NWs to undergo further reaction with Ni and phase transformation. Fast Ni diffusion was also observed in Si NWs, and continuous Ni diffusion could lead to the successive formation of multiple nickel silicide phases and transformation between them.[51] Annealing our as-grown samples at a higher temperature of 500 °C for 2 h in helium atmosphere (flow rate 8 sccm, pressure 4 Torr) resulted in little obvious morphological change (Figure 5a), although some surface roughening was occasionally observed in some NWs (Figure S5, Supporting Information). However, the NW phase is transformed from the orthorhombic NiGe phase to a hexagonal ε-Ni_5Ge_3 phase (space group

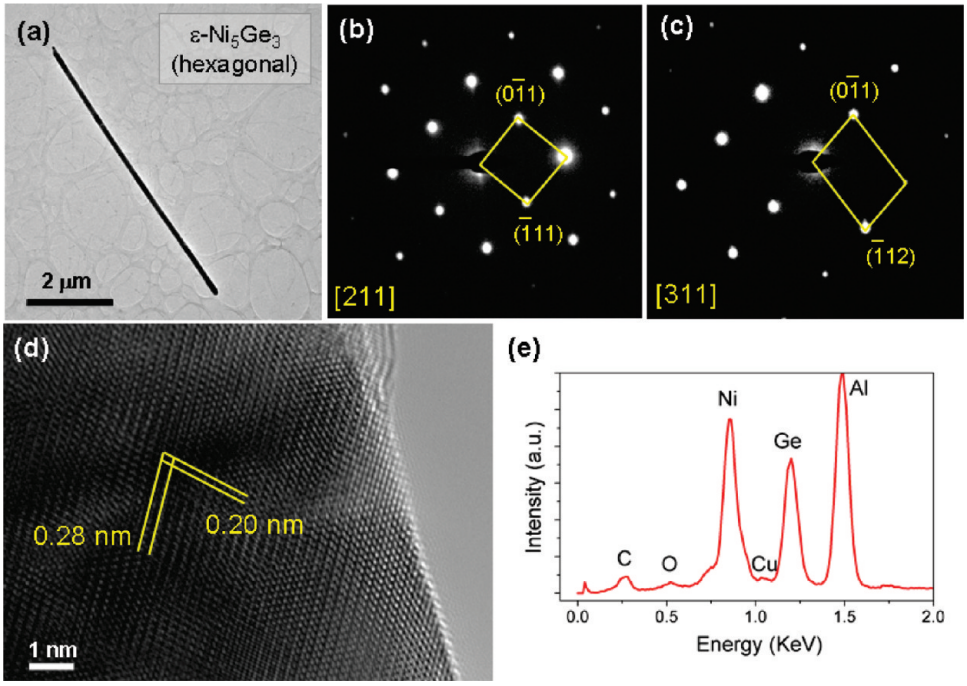

Figure 5. Structural characterization of the annealed nickel germanide NWs with hexagonal ε-Ni_5Ge_3 phase. (a) Low-magnification TEM image; ED patterns taken from the (b) [211] and (c) [311] zone axes; (d) HRTEM image; and (e) EDS spectrum of the ε-Ni_5Ge_3 NWs.

*P*6$_3$/*mmc*; a = 3.913 Å, c = 5.064 Å) by annealing.[52] XRD patterns from the annealed samples (Figure 4b) reveal significant contribution from a hexagonal ε-Ni_5Ge_3 phase (Figure 4a) along with some Ni, NiGe, Ni_2Ge (orthorhombic, space group *Pnma*; a = 5.11 Å, b = 3.83 Å, c = 7.26 Å), and Ni_3Ge (cubic, space group $Pm\bar{3}m$; a = 3.57 Å) phases (Figure S4, Supporting Information). To explicitly identify the NW phase, we studied a number of NWs using ED and HRTEM. The ED patterns of the annealed NWs (Figure 5b,c) are clearly in agreement with the hexagonal ordering expected from ε-Ni_5Ge_3 structures. The ED patterns can be readily indexed to the [211] and [311] zone axes of the hexagonal B8 ε-Ni_5Ge_3 parent structure ($a \sim 4$ Å and $c \sim 5$ Å).[35] The ED patterns and the lattice-resolved HRTEM image (Figure 5d) show that the ε-Ni_5Ge_3 NWs are single-crystalline (the surface oxide was partially removed when exposed to the convergent TEM electron beam, as shown in Figure S6, Supporting Information). Measured lattice spacings of 0.20 and 0.28 nm (from both the calibrated ED pattern and HRTEM image) correspond to the expected lattice spacing between the ($\bar{1}$12) and (0$\bar{1}$1) planes of the hexagonal ε-Ni_5Ge_3 phase, respectively. Importantly, we observed no evidence of superstructure reflections in the ED patterns of any wires examined, which would have suggested the monoclinic ε'-Ni_5Ge_3 and $Ni_{19}Ge_{12}$ phases. Furthermore, EDS spectra of individual annealed NWs (Figure 5e) show the Ni:Ge signal intensity ratio to be higher than that observed for the as-grown NWs (Figure 3e), indicating a higher Ni concentration in the annealed NWs. Quantitative EDS analyses on eight annealed NWs revealed an average Ni atomic percent of 67.7 $\pm$ 0.8%. The combination of all of our analysis results, including XRD, ED, HRTEM, and EDS, verifies that the annealed NWs possess the metastable B8 phase of hexagonal ε-Ni_5Ge_3.[52]

Direct evidence of phase transformation is further provided by the heterostructured ε-Ni_5Ge_3/NiGe NWs obtained by annealing for a shorter period (30 min). A clear interface between the ε-Ni_5Ge_3 and NiGe segments (indicated by red arrow) can be observed in such a typical heterostructured NW (Figure 6a). ED analysis verified that the NW tip was of NiGe phase (Figure S7, Supporting Information), which is consistent with the Ni diffusion mechanism. HRTEM image of the interfacial region (Figure 6b) clearly shows the different crystal lattices of ε-Ni_5Ge_3 and NiGe segments. The observation of this intermediate state of ε-Ni_5Ge_3/NiGe heterostructures provides direct view and solid evidence for the diffusion-induced phase transformation processes.

We further compare this work with previous reports on nickel germanide thin film synthesis, which mainly focused on the reactions of Ni thin film with Ge substrates ("Ni-on-Ge"), as opposed to the "Ge-on-Ni" reaction in our studies. Four phases (Ni, ε'-Ni_5Ge_3, NiGe, and minor Ge) were detected in as-grown samples, and five phases (Ni, Ni_3Ge, Ni_2Ge, ε-Ni_5Ge_3, and NiGe) were detected in annealed samples (Figure S4, Supporting Information) on the basis of PXRD. However, we would like to stress that our TEM, ED, and EDS analyses

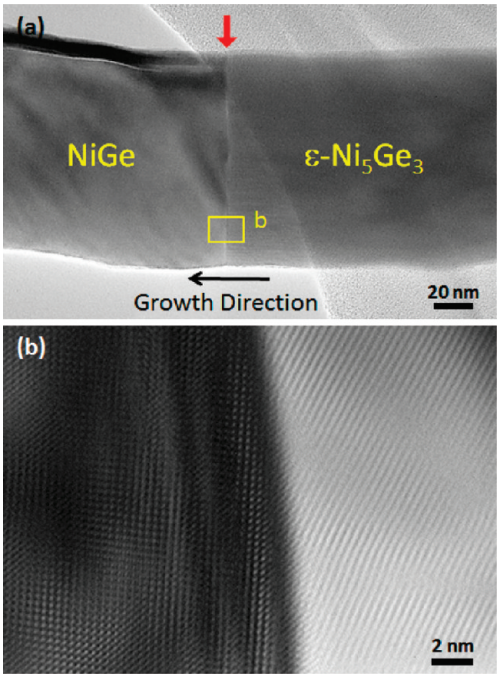

Figure 6. (a) TEM image of a heterostructured ε-Ni_5Ge_3/NiGe NW. The interface is indicated by a red arrow. (b) HRTEM image of the ε-Ni_5Ge_3/NiGe interfacial region.

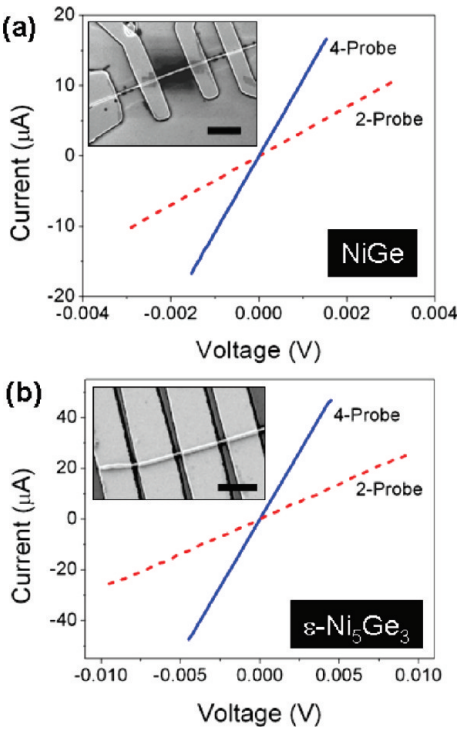

Figure 7. *I*−*V* characteristics (two-probe and four-probe) of representative (a) NiGe and (b) ε-Ni_5Ge_3 NW devices. Inset shows representative SEM images of the NW devices. Scale bars are 2 μm.

(Figure S8, Supporting Information) consistently show that the observed NWs are purely of NiGe and ε-Ni_5Ge_3 for as-grown and appropriately annealed samples, respectively. The other phases detected in XRD are from the underlying germanide films (Figure S9, Supporting Information). The phase formation sequence observed in previous thin film studies provides clues as to why such germanide phases and NWs of certain germanide phases were observed in our case. In the Ge-abundant Ni-on-Ge reactions of previous reports, NiGe (the most Ge-rich phase) was found to be the final stable phase.[1,8,12] Here, NiGe NWs were first obtained because it is the stable phase in the initial Ge-rich CVD growth conditions,[12] as reinforced by the observation of unreacted elemental Ge in the XRD patterns. However, in the overall Ni-abundant Ge-on-Ni reactions in our studies, Ni-rich phases (such as Ni_3Ge and Ni_2Ge) could eventually form after annealing (Figure S9). Given sufficient reaction time to reach equilibrium, the final phases depend on the identity and amount of the limiting reactant species. Thermal annealing leads to Ni enrichment and hence NW phase transformation to ε-Ni_5Ge_3.[11,53] However, the formation of the metastable hexagonal ε-Ni_5Ge_3 phase instead of the stable monoclinic ε'-Ni_5Ge_3 phase likely occurred due to the particular annealing conditions used, namely heating above the phase transition between the equilibrium phase and the metastable phases, annealing for the particular period, and relatively fast quenching. The observation of the metastable ε-Ni_5Ge_3 phase suggests that kinetic factors play important roles during phase transformation. We expect that variations in these annealing conditions could form different Ni_5Ge_3 structures, and it might be possible to further increase the Ni concentration, giving rise to Ni_2Ge or Ni_3Ge; however, we have not yet pursued this line of investigation.

Furthermore, we have characterized the electrical properties of the NiGe and ε-Ni_5Ge_3 NWs. The linear two-probe and four-probe *I*−*V* curves for both NiGe NW (Figure 7a) and ε-Ni_5Ge_3 NW (Figure 7b) devices indicate Ohmic behavior. The NW resistivities, ρ, were calculated using $\rho = RA/l$, where R is the measured resistance, A is the cross-sectional area of the NW (assumed to be circular in our case), and l is the channel length. With a diameter of 90.5 nm and a channel length of 2.57 μm (Figure 7a, inset), the room temperature resistivity of this representative NiGe NW was calculated to be 72 $\mu\Omega\cdot$cm for the two-probe measurement and 23 $\mu\Omega\cdot$cm for the four-probe measurement, indicating that the contact resistance is comparable to the device resistance. Measurements from a total of eight NiGe NWs revealed an average four-probe resistivity of 35 $\pm$ 15 $\mu\Omega\cdot$cm. This low four-probe resistivity is comparable to the reported values of 17−24 $\mu\Omega\cdot$cm for thin film NiGe samples[7,8] and also comparable to that of metal silicide contacts (NiSi, $CoSi_2$, and $TiSi_2$) commonly used in current Si microelectronics.[8,29,54] For the ε-Ni_5Ge_3 NWs shown in Figure 7b with a diameter of 117.2 nm and a device

channel length of 432 nm, the calculated resistivity is 906 $\mu\Omega\cdot$cm for the two-probe measurement and 234 $\mu\Omega\cdot$cm for the four-probe measurement. Additional measurements from a total of three ε-Ni_5Ge_3 NWs revealed an average four-probe resistivity of 132 ± 89 $\mu\Omega\cdot$cm, which is around 4 times of that for NiGe NWs. This is, to the best of our knowledge, the first electrical property study of the ε-Ni_5Ge_3 phase, probably due to its thermodynamic instability. The distinct properties of NiGe and ε-Ni_5Ge_3 NWs also underscore the importance of understanding the phase formation and evolution behavior of nanoscale germanides. For example, NiGe NWs may serve as excellent device contacts and/or interconnects due to their low resistivity. However, without careful processing control, the ε-Ni_5Ge_3 phase may potentially form, which is much more resistive, resulting in a significant increase in series resistance and performance degradation.

CONCLUSION

In conclusion, we have reported the spontaneous growth and phase transformation of nickel germanide NWs along with measurement of their electrical properties. The growth conditions were carefully optimized to grow NWs of uniform diameter in high density on porous Ni foam substrates. The as-grown NWs were found to be NiGe with orthorhombic crystal structure. Phase transformation from orthorhombic NiGe to hexagonal ε-Ni_5Ge_3 was achieved by thermal annealing induced Ni enrichment. Resistivity measurements revealed that the NiGe NWs were highly conductive (35 ± 15 $\mu\Omega\cdot$cm), but the resistivity of the ε-Ni_5Ge_3 NWs was much higher. Our studies demonstrate a facile and efficient method for nickel germanide NW synthesis and phase control. Understanding the germanide NW phase formation and transformation is of great importance for their applications in nanoelectronics due to the structure-dependent properties.

METHODS

Nanowire Growth and Transformation. The Ni germanide NWs were grown in a home-built CVD system composed of a horizontal quartz tube furnace with pressure and flow gas control. Porous Ni foam substrates were sonicated in 5% HCl for 15 min, rinsed with deionized (DI) water, and dried with N_2 gas before they were placed at the center of the tube furnace for NW growth. The tube chamber was purged with He gas during temperature ramping process; the flow gas was then switched to GeH_4 (10% diluted in He, 7−50 sccm) once the temperature had reached the set point. After a typical growth period of 2 h, the furnace was allowed to cool to room temperature naturally. NWs grew spontaneously from the Ni foam substrates in these CVD reactions without the use of an intentional catalyst. The best NW morphology was obtained at a growth temperature of 350 °C and a pressure of 4 Torr. To convert the NW further to the ε-Ni_5Ge_3 phase, the as-grown NWs were further annealed at 500 °C for 2 h in He atmosphere using the same CVD setup.

Characterizations. Morphologies of the products were characterized using SEM (LEO 1530). PXRD data were collected using Siemens STOE with Cu Kα radiation (λ = 1.5418 Å) on as-grown samples. Detailed structural characterizations of the NWs were performed using TEM (Philips CM200 and JEOL 2100F). Chemical compositions of the NWs were analyzed using EDS attached to the SEM system. For TEM and EDS analyses, the NWs were dispersed in isopropyl alcohol (IPA) by ultrasonication and then dropped on a Cu grid coated with lacey carbon film.

Device Fabrication and Measurements. To fabricate NW devices, the NW suspensions were dispersed on Si/SiO_2 (600 nm oxide) substrates and dried with N_2. The substrates are prepatterned with markers for NW location. Electrodes were defined by electron beam lithography. After a 15 s etching in buffered HF to remove surface oxide, Ti/Au (50/60 nm or 50/200 nm) electrodes were deposited using e-beam evaporation. Room temperature $I-V$ measurements were conducted using a Cascade Microtech RF-1 probing station and a custom computerized transport setup.

Acknowledgment. C.Y.Y. thanks NTU for research scholarship. J.M.H. and S.J. thank the NSF (CBET 1048625), University of Wisconsin—Madison graduate school, and the Sloan Research Fellowship for support. M.S.F. also thanks the NSF Graduate Research Fellowship for support.

Supporting Information Available: Additional materials as mentioned in the text. This material is available free of charge *via* the Internet at http://pubs.acs.org.

REFERENCES AND NOTES

1. Brunco, D. P.; De Jaeger, B.; Eneman, G.; Mitard, J.; Hellings, G.; Satta, A.; Terzieva, V.; Souriau, L.; Leys, F. E.; Pourtois, G.; *et al.* Germanium MOSFET Devices: Advances in Materials Understanding, Process Development, and Electrical Performance. *J. Electrochem. Soc.* **2008**, *155*, H552–H561.
2. Assefa, S.; Xia, F. N.; Vlasov, Y. A. Reinventing Germanium Avalanche Photodetector for Nanophotonic On-Chip Optical Interconnects. *Nature* **2010**, *464*, 80–85.
3. Zaima, S.; Nakatsuka, O.; Kondo, H.; Sakashita, M.; Sakai, A.; Ogawa, M. Silicide and Germanide Technology for Contacts and Gates in MOSFET Applications. *Thin Solid Films* **2008**, *517*, 80–83.
4. Choi, J.; Lim, D. K.; Kim, Y.; Kim, S. Structural and Electronic Properties of Cobalt Germanide Islands on Ge(100). *J. Phys. Chem. C* **2010**, *114*, 8992–8996.
5. Burchhart, T.; Lugstein, A.; Hyun, Y. J.; Hochleitner, G.; Bertagnolli, E. Atomic Scale Alignment of Copper–Germanide Contacts for Ge Nanowire Metal Oxide Field Effect Transistors. *Nano Lett.* **2009**, *9*, 3739–3742.
6. Simoen, E.; Opsomer, K.; Claeys, C.; Maex, K.; Detavernier, C.; Van Meirhaeghe, R. L.; Clauws, P. Study of Metal-Related Deep-Level Defects in Germanide Schottky Barriers on n-Type Germanium. *J. Appl. Phys.* **2008**, *104*, 023705/1–023705/7.
7. Gaudet, S.; Detavernier, C.; Kellock, A. J.; Desjardins, P.; Lavoie, C. Thin Film Reaction of Transition Metals with Germanium. *J. Vac. Sci. Technol., A* **2006**, *24*, 474–485.
8. Spann, J. Y.; Anderson, R. A.; Thornton, T. J.; Harris, G.; Thomas, S. G.; Tracy, C. Characterization of Nickel Germanide Thin Films for Use as Contacts to p-Channel Germanium MOSFETs. *IEEE Electron Device Lett.* **2005**, *26*, 151–153.
9. Xiang, J.; Lu, W.; Hu, Y. J.; Wu, Y.; Yan, H.; Lieber, C. M. Ge/Si Nanowire Heterostructures as High-Performance Field-Effect Transistors. *Nature* **2006**, *441*, 489–493.
10. Lu, W.; Xiang, J.; Timko, B. P.; Wu, Y.; Lieber, C. M. One-Dimensional Hole Gas in Germanium/Silicon Nanowire

Heterostructures. *Proc. Natl. Acad. Sci. U.S.A.* **2005**, *102*, 10046–10051.
11. Nash, A.; Nash, P. The Ge–Ni (Germanium–Nickel) System. *Bull. Alloy Phase Diagrams* **1987**, *8*, 255–264.
12. Nemouchi, F.; Mangelinck, D.; Bergman, C.; Clugnet, G.; Gas, P.; Labar, J. L. Simultaneous Growth of Ni_5Ge_3 and NiGe by Reaction of Ni Film with Ge. *Appl. Phys. Lett.* **2006**, *89*, 131920/1–131920/3.
13. Schmitt, A. L.; Higgins, J. M.; Szczech, J. R.; Jin, S. Synthesis and Applications of Metal Silicide Nanowires. *J. Mater. Chem.* **2010**, *20*, 223–235.
14. Kim, C. J.; Kang, K.; Woo, Y. S.; Ryu, K. G.; Moon, H.; Kim, J. M.; Zang, D. S.; Jo, M. H. Spontaneous Chemical Vapor Growth of NiSi Nanowires and Their Metallic Properties. *Adv. Mater.* **2007**, *19*, 3637–3642.
15. Yoon, H.; Seo, K.; Bagkar, N.; In, J.; Park, J.; Kim, J.; Kim, B. Vertical Epitaxial Co_5Ge_7 Nanowire and Nanobelt Arrays on a Thin Graphitic Layer for Flexible Field Emission Displays. *Adv. Mater.* **2009**, *21*, 4979–4982.
16. Higgins, J. M.; Schmitt, A. L.; Guzei, I. A.; Jin, S. Higher Manganese Silicide Nanowires of Nowotny Chimney Ladder Phase. *J. Am. Chem. Soc.* **2008**, *130*, 16086–16094.
17. Zhou, F.; Szczech, J.; Pettes, M. T.; Moore, A. L.; Jin, S.; Shi, L. Determination of Transport Properties in Chromium Disilicide Nanowires *via* Combined Thermoelectric and Structural Characterizations. *Nano Lett.* **2007**, *7*, 1649–1654.
18. Schmitt, A. L.; Higgins, J. M.; Jin, S. Chemical Synthesis and Magnetotransport of Magnetic Semiconducting $Fe_{1-x}Co_x$-Si Alloy Nanowires. *Nano Lett.* **2008**, *8*, 810–815.
19. Higgins, J. M.; Ding, R. H.; DeGrave, J. P.; Jin, S. Signature of Helimagnetic Ordering in Single-Crystal MnSi Nanowires. *Nano Lett.* **2010**, *10*, 1605–1610.
20. Liao, L.; Lin, Y. C.; Bao, M.; Cheng, R.; Bai, J.; Liu, Y.; Qu, Y.; Wang, K. L.; Huang, Y.; Duan, X. High-Speed Graphene Transistors with a Self-Aligned Nanowire Gate. *Nature* **2010**, *467*, 305–308.
21. Nash, P.; Nash, A. The Ni–Si (Nickel–Silicon) System. *Bull. Alloy Phase Diagrams* **1987**, *8*, 6–14.
22. Lee, C. Y.; Lu, M. P.; Liao, K. F.; Lee, W. F.; Huang, C. T.; Chen, S. Y.; Chen, L. J. Free-Standing Single-Crystal $NiSi_2$ Nanowires with Excellent Electrical Transport and Field Emission Properties. *J. Phys. Chem. C* **2009**, *113*, 2286–2289.
23. Lu, K. C.; Wu, W. W.; Wu, H. W.; Tanner, C. M.; Chang, J. P.; Chen, L. J.; Tu, K. N. *In Situ* Control of Atomic-Scale Si Layer with Huge Strain in the Nanoheterostructure NiSi/Si/NiSi through Point Contact Reaction. *Nano Lett.* **2007**, *7*, 2389–2394.
24. Kim, J.; Anderson, W. A. Spontaneous Nickel Monosilicide Nanowire Formation by Metal Induced Growth. *Thin Solid Films* **2005**, *483*, 60–65.
25. Kang, K.; Kim, S. K.; Kim, C. J.; Jo, M. H. The Role of NiO_x Overlayers on Spontaneous Growth of $NiSi_x$ Nanowires From Ni Seed Layers. *Nano Lett.* **2008**, *8*, 431–436.
26. Sun, Z. Q.; Whang, S. J.; Yang, W. F.; Lee, S. J. Synthesis of Nickel Mono-Silicide Nanowire by Chemical Vapor Deposition on Nickel Film: Role of Surface Nickel Oxides. *Jpn. J. Appl. Phys.* **2009**, *48*, 04C138/1–04C138/8.
27. Kim, J.; Shin, D. H.; Lee, E. S.; Han, C. S.; Park, Y. C. Electrical Characteristics of Single and Doubly Connected Ni Silicide Nanowire Grown by Plasma-Enhanced Chemical Vapor Deposition. *Appl. Phys. Lett.* **2007**, *90*, 253103/1–253103/3.
28. Liu, Z. H.; Zhang, H.; Wang, L.; Yang, D. R. Controlling the Growth and Field Emission Properties of Silicide Nanowire Arrays by Direct Silicification of Ni Foil. *Nanotechnology* **2008**, *19*, 375602/1–375602/4.
29. Song, Y. P.; Schmitt, A. L.; Jin, S. Ultralong Single-Crystal Metallic Ni_2Si Nanowires with Low Resistivity. *Nano Lett.* **2007**, *7*, 965–969.
30. Yan, X. Q.; Yuan, H. J.; Wang, J. X.; Liu, D. F.; Zhou, Z. P.; Gao, Y.; Song, L.; Liu, L. F.; Zhou, W. Y.; Wang, G.; *et al.* Synthesis and Characterization of a Large Amount of Branched Ni_2Si Nanowires. *Appl. Phys. A* **2004**, *79*, 1853–1856.
31. Lee, C. Y.; Lu, M. P.; Liao, K. F.; Wu, W. W.; Chen, L. J. Vertically Well-Aligned Epitaxial $Ni_{31}Si_{12}$ Nanowire Arrays with Excellent Field Emission Properties. *Appl. Phys. Lett.* **2008**, *93*, 113109/1–113109/3.
32. Song, Y. P.; Jin, S. Synthesis and Properties of Single-Crystal β_3-Ni_3Si Nanowires. *Appl. Phys. Lett.* **2007**, *90*, 173122/1–173122/3.
33. Kim, J.; Lee, E. S.; Han, C. S.; Kang, Y.; Kim, D.; Anderson, W. A. Observation of Ni Silicide Formations and Field Emission Properties of Ni Silicide Nanowires. *Microelectron. Eng.* **2008**, *85*, 1709–1712.
34. *ASM Binary Alloy Phase Diagram*, CD-ROM; ASM international: Materials Park, OH.
35. Larsson, A. K.; Withers, R. An Electron Diffraction Study of Modulated $Ni_{1+x}Ge$ B8 Type Phases. *J. Alloys Compd.* **1998**, *264*, 125–132.
36. Lensch-Falk, J. L.; Hemesath, E. R.; Lauhon, L. J. Syntaxial Growth of Ge/Mn-Germanide Nanowire Heterostructures. *Nano Lett.* **2008**, *8*, 2669–2673.
37. Higgins, J. M.; Carmichael, P.; Schmitt, A. L.; Lee, S.; Degrave, J. P.; Jin, S. Mechanistic Investigation of the Growth of $Fe_{1-x}Co_xSi$ ($0 \leq x \leq 1$) and $Fe_5(Si_{1-y}Ge_y)_3$ ($0 \leq y \leq 0.33$) Ternary Alloy Nanowires. *ACS Nano* **2011**, *5*, 3268–3277.
38. Szczech, J. R.; Jin, S. Epitaxially-Hyperbranched FeSi Nanowires Exhibiting Merohedral Twinning. *J. Mater. Chem.* **2010**, *20*, 1375–1382.
39. Zhang, H. L.; Li, F.; Liu, C.; Cheng, H. M. The Facile Synthesis of Nickel Silicide Nanobelts and Nanosheets and Their Application in Electrochemical Energy Storage. *Nanotechnology* **2008**, *19*, 165606/1–165606/7.
40. Wang, D. W.; Dai, H. J. Low-Temperature Synthesis of Single-Crystal Germanium Nanowires by Chemical Vapor Deposition. *Angew. Chem., Int. Ed.* **2002**, *41*, 4783–4786.
41. Kamins, T. I.; Li, X.; Williams, R. S. Growth and Structure of Chemically Vapor Deposited Ge Nanowires on Si Substrates. *Nano Lett.* **2004**, *4*, 503–506.
42. Woodruff, J. H.; Ratchford, J. B.; Goldthorpe, I. A.; McIntyre, P. C.; Chidsey, C. E. D. Vertically Oriented Germanium Nanowires Grown From Gold Colloids on Silicon Substrates and Subsequent Gold Removal. *Nano Lett.* **2007**, *7*, 1637–1642.
43. Dubois, L. H.; Nuzzo, R. G. The Decomposition of Silane and Germane on Ni(111): Implications for Heterogeneous Catalysis. *Surf. Sci.* **1985**, *149*, 133–145.
44. Claeys, C. L.; Simoen, E. *Germanium-Based Technologies: From Materials to Devices*; Elsevier Science Ltd.: Amsterdam, 2007.
45. Lensch-Falk, J. L.; Hemesath, E. R.; Perea, D. E.; Lauhon, L. J. Alternative Catalysts for VSS Growth of Silicon and Germanium Nanowires. *J. Mater. Chem.* **2009**, *19*, 849–857.
46. Seo, K.; Yoon, H.; Ryu, S. W.; Lee, S.; Jo, Y.; Jung, M. H.; Kim, J.; Choi, Y. K.; Kim, B. Itinerant Helimagnetic Single-Crystalline MnSi Nanowires. *ACS Nano* **2010**, *4*, 2569–2576.
47. Bierman, M. J.; Lau, Y. K. A.; Kvit, A. V.; Schmitt, A. L.; Jin, S. Dislocation-Driven Nanowire Growth and Eshelby Twist. *Science* **2008**, *320*, 1060–1063.
48. Jin, S.; Bierman, M. J.; Morin, S. A. A New Twist on Nanowire Formation: Screw-Dislocation-Driven Growth of Nanowires and Nanotubes. *J. Phys. Chem. Lett.* **2010**, *1*, 1472–1480.
49. Morin, S. A.; Bierman, M. J.; Tong, J.; Jin, S. Mechanism and Kinetics of Spontaneous Nanotube Growth Driven by Screw Dislocations. *Science* **2010**, *328*, 476–480.
50. Yan, C. Y.; Singh, N.; Lee, P. S. Morphology Control of Indium Germanate Nanowires, Nanoribbons, and Hierarchical Nanostructures. *Cryst. Growth Des.* **2009**, *9*, 3697–3701.
51. Lin, Y. C.; Chen, Y.; Xu, D.; Huang, Y. Growth of Nickel Silicides in Si and Si/SiO_x Core/Shell Nanowires. *Nano Lett.* **2010**, *10*, 4721–4726.
52. The "Ni_5Ge_3" phase field encompasses the nominal compositions of ε'-Ni_5Ge_3, ε-Ni_5Ge_3, Ni_3Ge_2, and $Ni_{19}Ge_{12}$. As related structures intermediate between the NiAs and Ni_2In archetypal structure types, they are sometimes referred to as B8 structures and differ only from these archetypes by the partial filling of trigonal bipyramidal interstitial sites and the resulting long-range order and

structural relaxation. These structures maintain the same parent archetype, but it is difficult to distinguish these structures by PXRD without additional information. The complex superstructures exhibited by ε'-Ni_5Ge_3 and $Ni_{19}Ge_{12}$ as a result of the long-range ordering of these vacancies can distinguish these two through single-crystal XRD and ED experiments. Ni_3Ge_2 and ε-Ni_5Ge_3 have disordered arrangements of the remaining vacancies and so exhibit nearly identical diffraction behavior from the parent lattice, but they can be distinguished by chemical compositions. Careful analysis of the "Ni_5Ge_3" nanowires by combining several techniques can lead to the identification of the particular B8 phase, which was done in the case at hand.

53. Jensen, J. M.; Ly, S.; Johnson, D. C. Low-Temperature Preparation of High-Temperature Nickel Germanides Using Multilayer Reactants. *Chem. Mater.* **2003**, *15*, 4200–4204.
54. Seger, J.; Zhang, S. L.; Mangelinck, D.; Radamson, H. H. Increased Nucleation Temperature of $NiSi_2$ in the Reaction of Ni Thin Films with $Si_{1-x}Ge_x$. *Appl. Phys. Lett.* **2002**, *81*, 1978–1980.